

Data set diagonalization in a global fit

Jon Pumplin

Michigan State University, East Lansing MI 48824, USA

(Dated: February 21, 2024)

The analysis of data sometimes requires fitting many free parameters in a theory to a large number of data points. Questions naturally arise about the compatibility of specific subsets of the data, such as those from a particular experiment or those based on a particular technique, with the rest of the data. Questions also arise about which theory parameters are determined by specific subsets of the data. I present a method to answer both of these kinds of questions. The method is illustrated by applications to recent work on measuring parton distribution functions.

1. INTRODUCTION

There are many situations where data from a variety of different experiments must be fitted to a single underlying theory that has many free parameters. The particular instance that led to this work is the measurement of parton distribution functions (PDFs), which describe momentum distributions of quarks and gluons in the proton [1, 2, 3, 4, 5].

In these situations, it would be desirable to assess the consistency between the full body of data and individual subsets of it, such as data from a particular experiment, or data that rely on a particular technique, or data in which a particular kind of theoretical or experimental systematic error is suspected. It would also be desirable to characterize which parameters in the fit are determined by particular components of the input data. This paper presents a "Data Set Diagonalization" (DSD) procedure that answers both of those desires.

2. NEW EIGENVECTOR METHODS

The quality of the fit of a theory to a set of data is measured by a quantity χ^2 , which in simplest form is given by

$$\chi^2 = \sum_{i=1}^N \frac{(D_i - T_i)^2}{E_i}; \quad (1)$$

where D_i and E_i represent a data point and its uncertainty, and T_i is the theoretical prediction. (Although (1) is standard practice, some alternatives might be worth consideration [6].)

The predictions T_i in Eq. (1) depend on a number of parameters $a_1; \dots; a_N$. The best-fit estimate for those parameters is obtained by adjusting them to minimize χ^2 . The uncertainty range is estimated as the neighborhood of the minimum in which χ^2 lies within a

certain "tolerance criterion" χ^2 above its minimum value. If the errors in the data are random and Gaussian with standard deviations truly given by E_i , and the theory is without error, the appropriate χ^2 can be related to confidence intervals by standard statistical methods. Those premises do not hold in the application of interest here; but the tolerance range can be estimated by examining the stability of the fit in response to applying different weights to subsets of the data [1, 2, 7].

Sufficiently close to its minimum, χ^2 is an approximately quadratic function of the parameters $a_1; \dots; a_N$. Using the eigenvectors of the matrix that defines that quadratic form as basis vectors in the N -dimensional parameter space, one can define new theory parameters $z_1; \dots; z_N$ which are linear combinations of the original ones

$$a_i = a_i^{(0)} + \sum_{j=1}^N W_{ij} z_j; \quad (2)$$

and which transform χ^2 into the very simple form

$$\chi^2 = \chi_{\min}^2 + \sum_{i=1}^N z_i^2; \quad (3)$$

Formally, the transformation matrix W can be computed by evaluating the Hessian matrix $\partial^2 \chi^2 / \partial a_i \partial a_j$ at the minimum using finite differences, and computing its eigenvectors. The new parameters z_i are then just coefficients that multiply those eigenvectors when the original coordinates $a_1; \dots; a_N$ are expressed as linear combinations of them. In the PDF application, this straightforward procedure breaks down because the eigenvalues of the Hessian span a huge range of magnitudes, which makes non-quadratic behavior complicate the finite-difference method at very different scales for different directions in parameter space. However, this difficulty can be overcome by an iterative technique [1] that is reviewed in the Appendix.

The linear transformation (2) that leads to (3) is not unique, since any further orthogonal transform of the

coordinates z_i will preserve that form. Such an orthogonal transformation can be defined using the eigenvectors of any symmetric matrix. After this second linear transformation of the coordinates, the chosen symmetric matrix will be diagonal together with χ^2 . The second transformation can be combined with the first to yield a single overall linear transformation of the form (2). Thus there is a freedom to diagonalize an additional symmetric matrix while maintaining the simple form (3) for χ^2 .

That symmetric matrix can be taken from the matrix of second derivatives that appears when the variation of any function of the fitting parameters is expanded in Taylor series through second order. Thus it is possible within the quadratic approximation to diagonalize any one chosen function of the fitting parameters, while maintaining the diagonal form for χ^2 . An explicit recipe for this "rediagonalization" procedure is given in the Appendix.

The freedom to diagonalize an additional quantity along with χ^2 can be exploited in several ways:

1. The traditional approach in which one only diagonalizes the Hessian matrix is formally equivalent to also diagonalizing the displacement distance D from the minimum point in the space of the original fitting parameters:

$$D^2 = \sum_{i=1}^N (a_i - a_i^{(0)})^2 : \quad (4)$$

In this approach, the natural eigenvectors can usefully be ordered by their eigenvalues, from "steep" directions in which χ^2 rises rapidly with D , to "flat" directions in which χ^2 varies very slowly with D . This option has been used in the iterative method that was developed for previous CTEQ PDF error analyses [8].

2. One can diagonalize the contribution to χ^2 from any chosen subset S of the data. This option is the basis of the DSD procedure, which is described in the next Section and applied in the rest of the paper.

3. One can diagonalize some quantity G that is of particular theoretical interest, such as the prediction for some unmeasured quantity. In this way, one might find that a small subset of the eigenvectors is responsible for most of the range of possibilities for that prediction, which would simplify the application of the Hessian method. An example of this was given in a recent PDF study [4]. However, there is no guarantee in general that the diagonal form will be dominated by

a few directions with large coefficients (α_i and/or β_i in Eq. (28) of the Appendix). Hence a better scheme to reduce the number of important eigenvectors might well be to simply choose the new z_1 along the gradient direction $\partial G = \partial z_i$, and then to choose the new z_2 along the orthogonal direction that carries the largest residual variation, etc.

3. THE DSD METHOD

Let us diagonalize the contribution χ_S^2 from some chosen subset S of the data. That puts its contribution to the total χ^2 into a diagonal form

$$\chi_S^2 = \sum_{i=1}^N (2\alpha_i z_i + \beta_i z_i^2) \quad (5)$$

while preserving (3), as is derived in the Appendix. The contribution $\chi_{\bar{S}}^2 = \chi^2 - \chi_S^2$ from the remainder of the data \bar{S} is then similarly diagonal.

If the parameters α_i all lie in the range $0 < \alpha_i < 1$, Eqs. (3) and (5) can be written in the form

$$\begin{aligned} \chi^2 &= \chi_S^2 + \chi_{\bar{S}}^2 \\ \chi_S^2 &= \text{const} + \sum_{i=1}^N \frac{z_i - A_i}{B_i}^2 \\ \chi_{\bar{S}}^2 &= \text{const} + \sum_{i=1}^N \frac{z_i - C_i}{D_i}^2 : \end{aligned} \quad (6)$$

These equations have an obvious interpretation that is the basis of the DSD method: In the new coordinates, the subset S of the data and its complement \bar{S} take the form of independent measurements of the N variables z_i in the quadratic approximation. The results from Eq. (6) can be read as

$$\begin{aligned} z_i &= A_i \pm B_i \text{ according to } S \\ z_i &= C_i \pm D_i \text{ according to } \bar{S} \end{aligned} \quad (7)$$

where

$$\begin{aligned} A_i &= \sum_{j=1}^P \alpha_j z_j^{(i)}; B_i = 1 - \sum_{j=1}^P \alpha_j^2 \\ C_i &= \sum_{j=1}^P \beta_j z_j^{(i)}; D_i = 1 - \sum_{j=1}^P \beta_j^2 : \end{aligned} \quad (8)$$

Eqs. (7)–(8) provide a direct assessment of the compatibility between the subset S and the rest of the data \bar{S} . For if Gaussian statistics can be used to combine the uncertainties in quadrature, the difference between

the two measurements of z_i is

$$\chi^2_i = \frac{A_i^2 + C_i^2}{B_i^2 + D_i^2} = \frac{1}{(1 - \alpha_i)} : \quad (9)$$

This leads to a chi-squared measure of the overall difference between S and \bar{S} along direction z_i :

$$\chi^2_i = \frac{A_i^2 + C_i^2}{B_i^2 + D_i^2} = \frac{1}{(1 - \alpha_i)} : \quad (10)$$

(The symmetry of (10) under the interchange $\alpha_i \leftrightarrow 1 - \alpha_i$ reflects the obvious symmetry $S \leftrightarrow \bar{S}$.) Even in applications where Gaussian statistics cannot be assumed, the variables z_i are natural quantities for testing the compatibility of S with the rest of the data.

Eqs. (7)–(8) also directly answer the question “How is measured by the subset S of data?”. For, provided S is compatible with its complement, the variables z_i that are significantly measured by S are those for which the uncertainty B_i from S is less than or comparable to the uncertainty D_i from \bar{S} .

α_i	$B_i = D_i$
0.9	1=3
0.8	1=2
0.5	1=1
0.2	2=1
0.1	3=1

TABLE I: Ratio between B_i = uncertainty from S and D_i = uncertainty from \bar{S} , for various α_i .

For purposes of orientation, the relationship between α_i and the ratio of uncertainties $B_i = D_i$ is shown in Table I for some values of α_i that correspond to simple ratios. In particular, $\alpha_i = 0.5$ means that S and \bar{S} contribute equally to the measurement of z_i ; while $\alpha_i = 0.9$ means that the uncertainty from S is three times smaller than from \bar{S} ; and $\alpha_i = 0.1$ means that the uncertainty from S is three times larger than from \bar{S} . Practically speaking, one can say that S dominates the measurement of z_i if $\alpha_i > 0.8$ – 0.9 , while the complementary set \bar{S} dominates if $\alpha_i < 0.1$ – 0.2 . Beyond those ranges, the contribution from the less-important quantity is strongly suppressed when the weighted average is taken.

Another way to interpret the α_i parameter is as follows. Pretend that S consists of N_S repeated measurements of z_i , each having the same precision; and that

\bar{S} similarly consists of $N_{\bar{S}}$ measurements. The ratio of uncertainties is then given by

$$\frac{B_i}{D_i} = \sqrt{\frac{N_{\bar{S}}}{N_S}} \Rightarrow \alpha_i = \frac{N_S}{N_S + N_{\bar{S}}} : \quad (11)$$

Thus α_i can be interpreted as the fraction of the data that is contained in subset S , for the purpose of measuring z_i .

In applications of the DSD method, it is likely that not all of the α_i parameters will lie in the range $0 < \alpha_i < 1$. For if $\alpha_i > 1$, then S dominates the measurement of z_i , so \bar{S} is quite insensitive to z_i , so the dependence of χ^2_S on z_i is likely not to be described well by a quadratic approximation. Similarly $\alpha_i < 0$ means that \bar{S} dominates the measurement of z_i , so the small dependence of $\chi^2_{\bar{S}}$ on z_i may not be very quadratic.

Compatibility between S and \bar{S} along directions for which $\alpha_i > 0.8$ or $\alpha_i < 0.2$ is not a crucial issue, since one or the other measurement dominates the average along such directions. It is an important feature of the DSD method that it distinguishes between inconsistencies that do or do not affect the overall fit. In that sense, it is a more sensitive tool than the previous method of simply studying χ^2_S vs. $\chi^2_{\bar{S}}$ by means of a variable weight [7].

4. APPLICATIONS TO PARTON DISTRIBUTION ANALYSIS

The interpretation of data from high energy colliders such as the Tevatron at Fermilab and the LHC at CERN relies on knowing the PDFs that describe momentum distributions of quarks and gluons in the proton. These PDFs are extracted by a “global analysis” [4, 5] of many kinds of experiments whose results are tied together by the theory of Quantum Chromodynamics (QCD). The analysis described here to illustrate the DSD method is based on 36 data sets with a total of 2959 data points. These are the same data sets used in a recent PDF analysis [4], except that two older inclusive jet experiments have been dropped for simplicity.

The theory uses the same 24 free parameters as that recent analysis. These parameters describe the momentum distributions $u(x)$, $d(x)$, $u(x)$, $d(x)$, $s(x)$ and $g(x)$ at a particular small QCD scale. All of the PDFs at higher scale can be calculated from these by QCD.

This PDF application is a strong test of the new method, because the large number of experiments of

different types carries the possibility for unknown experimental and theoretical systematic errors, and the large number of free parameters includes a wide range of flat and steep directions in parameter space.

4.1. E605 experiment

We first apply the data set diagonalization method to study the contribution of the E605 experiment [9] to the PDF analysis. This experiment (lepton pair production in proton scattering on copper) is sensitive to the various flavors of quarks in the proton in a different way from the majority of the data, so it can be expected to be responsible for one or more specific features of the global fit. It is also an experiment where unknown systematic errors might be present, since no corrections for possible nuclear target effects are included.

There are 24 free parameters in the fit, and hence 24 mutually orthogonal eigenvector directions. In descending order, the first 4 of these are found to have $\alpha_1 = 0.91$, $\alpha_2 = 0.38$, $\alpha_3 = 0.16$, $\alpha_4 = 0.06$. All of the other eigenvectors have still smaller or even negative α_i . Hence according to the previous discussion, the fit is controlled mainly by this E605 data set along eigenvector direction 1; E605 and its complement both play a role along direction 2; E605 plays a very minor role along direction 3; and it is unimportant along the remaining 21 directions.

This is confirmed in Fig. 1, which shows the variation of χ^2 , with the best-fit values subtracted, for E605 (119 data points) and its complement (the remaining 2840 data points) along each of the first four directions. A long direction 1, the E605 data indeed dominate the measurement: the "parabola" of χ^2_S is much narrower than the "parabola" of $\chi^2_{\bar{S}}$. The minimum for the complementary data set \bar{S} lies rather far from the best-fit value $z_1 = 0$, but its χ^2 is so slowly varying that it is not inconsistent with that value. A long direction 2, E605 and its complement are both important, and the two measures are again seen to be consistent with each other. For the remaining 2 directions shown, and the 20 directions that are not shown, the \bar{S} data completely dominate: E605 provides negligible information along those directions. (The z_4 curve for E605 ends abruptly, because the fit becomes numerically unphysical at that point, which is far outside the region of acceptable fits to \bar{S} .)

The S and \bar{S} columns of Table II show the information of Fig. 1 interpreted as measurements of z_1, \dots, z_4 . This can be done according to Eqs. (6)–(8), or more precisely by fitting each of the curves in

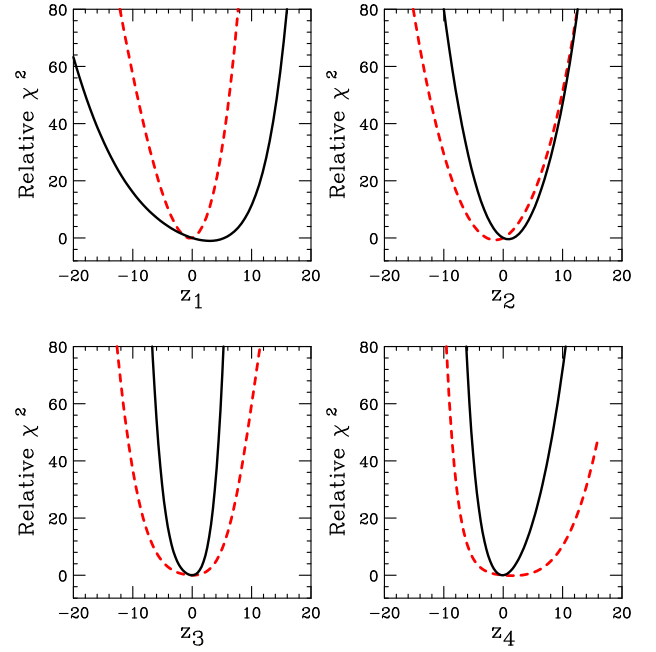


FIG. 1: χ^2 for fit to E605 (dashed curves) and to the rest of the data (solid curves) along the four leading eigenvector directions in descending order of α_i . In each panel, $z_i = 0$ is the location of the overall best fit.

i	α_i	z_i from S		z_i from \bar{S}		Difference		α_i
1	0.91	0.37	1.07	2.94	2.67	3.31	2.88	1.15
2	0.38	1.38	1.61	0.87	1.29	2.26	2.07	1.09
3	0.16	0.05	2.45	0.01	1.10	0.06	2.68	0.02
4	0.06	1.57	3.92	0.10	1.03	1.67	4.05	0.41

TABLE II: Consistency between $S =$ E605 experiment and $\bar{S} =$ the remainder of data.

Fig. 1 to a parabolic form in the neighborhood of its minimum rather than fitting at $z_i = 0$. The Difference column is the difference between the S and \bar{S} measurements of z_i , with an error estimate obtained by adding the S and \bar{S} errors in quadrature. The α column expresses this difference in units of its uncertainty, which would be the number of standard deviations for Gaussian statistics. The fact that these numbers are < 1 implies that the E605 experiment is consistent with the rest of the global analysis.

4.2. Inclusive jet experiments

We now turn our attention to the role of the CDF [10] and D0 [11] run II jet experiments in the PDF analysis. This was the principal subject of a recent paper [4]; but the DSD technique can shed new light on it. We first examine the consistency between each jet experiment and the rest of the data with the other jet experiment excluded. Results for the leading i are shown in Table III for CDF and Table IV for D0. The CDF experiment plays a strong role along its two leading directions ($z_1 = 0.75$ and $z_2 = 0.62$), showing a rather strong tension (3.6) along z_2 . The D0 experiment similarly plays a strong role along its two leading directions ($z_1 = 0.71$ and $z_2 = 0.52$), but it is consistent with the non-jet data along both of those directions.

i	z_i	z_i from S		z_i from \bar{S}		Difference		z_i
1	0.75	0.55	1.11	1.74	1.85	2.28	2.15	1.06
2	0.62	2.66	1.25	4.34	1.52	7.00	1.96	3.56
3	0.04	11.26	4.14	0.58	1.03	11.84	4.26	2.78

TABLE III: Consistency between $S = \text{CDF}$ and $\bar{S} = \text{all non-jet data}$.

i	z_i	z_i from S		z_i from \bar{S}		Difference		z_i
1	0.71	0.49	1.11	1.33	1.79	1.82	2.11	0.86
2	0.52	1.05	1.36	1.26	1.51	2.31	2.03	1.14
3	0.07	2.00	3.89	0.14	1.03	2.14	4.02	0.53

TABLE IV: Consistency between $S = \text{D0}$ and $\bar{S} = \text{all non-jet data}$.

Since these jet experiments measure the same process by similar techniques, it also makes sense to combine them into a single subset S . The result is given in Table V. The z_i parameters in descending order are $z_1 = 0.82$, $z_2 = 0.74$, $z_3 = 0.12$, $z_4 = 0.05$, so these data supply most of the constraint along their two leading directions, and negligible constraint along any of the others. The expectation that these two experiments measure the same thing is confirmed by the fact that there are still only two directions being determined, with z_1 and z_2 larger than for either experiment alone. Some tension (2.8) exists between S and \bar{S} along z_2 ; but combining the data sets has reduced the conflict relative to what appeared with CDF alone.

Figure 2 shows the variation in χ^2 for the fit to the jet data (72 + 110 points) and its complement (2777

i	z_i	z_i from S		z_i from \bar{S}		Difference		z_i
1	0.82	0.35	1.08	1.68	2.31	2.02	2.55	0.79
2	0.74	1.62	1.15	4.60	1.89	6.23	2.21	2.81
3	0.12	0.19	2.84	0.03	1.07	0.21	3.04	0.07
4	0.05	3.14	4.34	0.16	0.97	3.31	4.44	0.74

TABLE V: Consistency between $S = \text{CDF} + \text{D0 jet data}$ and $\bar{S} = \text{all non-jet data}$.

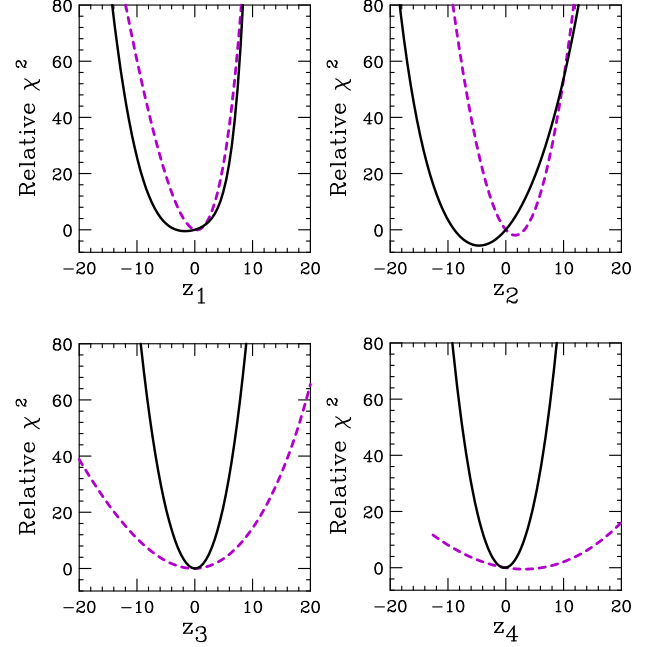


FIG. 2: χ^2 for fit to CDF+D0 (dashed curves) and to the remaining data (solid curves), for the four leading directions in descending order of z_i .

points) along the four leading directions. The numerical results shown in Table V correspond to fitting these curves by parabolas at their minima. For the first two directions, the "parabola" for the jet data S is narrower than the "parabola" for its complement, as expected since $z_1, z_2 > 0.5$. This confirms that the jet data dominate the global fit along those directions. For z_3 and z_4 (and all other directions, which are not shown), the jet data supply very little constraint: the "parabola" is much broader for S than for \bar{S} . The locations of the minima are quite far apart for z_2 , which reflects the tension between S and \bar{S} along that direction.

To study the consistency between the two individual jet experiments within the context of the global fit, their χ^2 values are plotted separately in Fig. 3 along

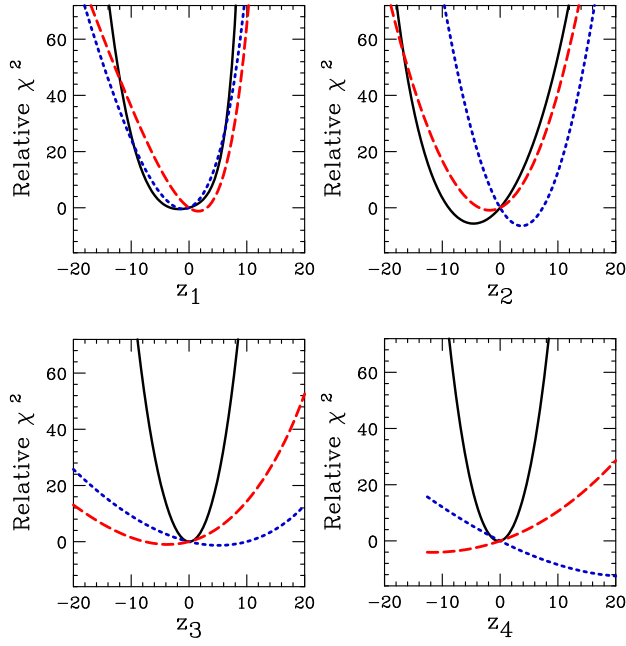


FIG. 3: χ^2 for jet experiments (dotted), D0 (dashed), and the rest of the data (solid).

the same eigenvector directions as in Fig. 2. There appears to be a bit of tension between the two experiments along these directions, since their minima occur at different places. Quantitatively, fitting each curve in Fig. 3 to a parabola near its minimum, leads to the results shown in Table VI. The discrepancy between the jet experiments is 2:4 and 1:6 along the two directions in which these experiments are significant in the global fit. Any discrepancy between the jet experiments along other directions, including the strong difference along direction 4, is not important for the global fit, because non-jet experiments supply much stronger constraints along those directions, as is confirmed by the narrow parabola for \bar{S} .

i	z_i from CDF	z_i from D0	Difference	χ^2_i
1	2:70 1:65	2:45 1:38	5:15 2:15	2:40
2	2:33 1:35	1:74 2:22	4:07 2:60	1:57

TABLE VI: Consistency between CDF and D0 jet experiments.

The DSD method can also be used to discover which aspects of a global fit are determined by particular subsets of the data. An example of this is illustrated by Fig. 4, which shows the gluon distribution at QCD scale 1:3 GeV, for PDF sets corresponding to displace-

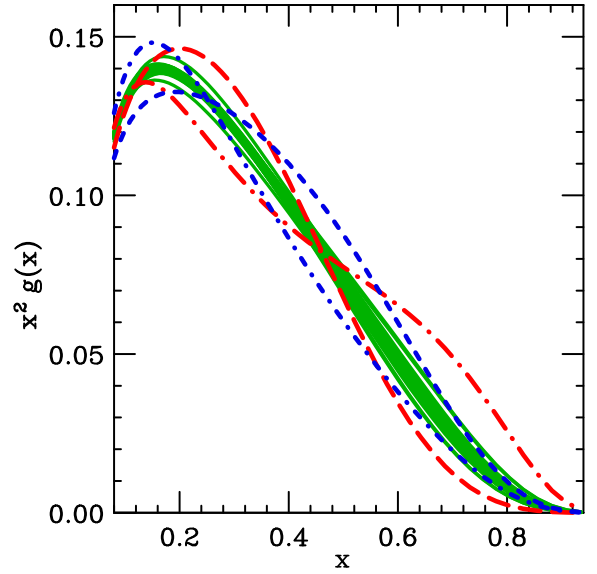


FIG. 4: Gluon distributions $g(x)$ at $z_1 = 4:0$ (long dash), $z_1 = -4:0$ (long dash dot), $z_2 = 4:0$ (short dash), $z_2 = -4:0$ (short dash dot), and $z_i = -4:0$ for $i = 3; \dots; 24$ (solid). Most of the uncertainty for $g(x)$ comes from eigenvector directions 1 and 2, which are controlled principally by the jet experiments according to Fig. 2.

ments $z_i = -4$ along each eigenvector direction of the CDF+D0 fit. Most of the uncertainty is seen to come from the z_1 and z_2 directions, which are the directions found above to be controlled by the jet data. This directly confirms the conclusion of [4] that the jet data are the major source of information about the gluon distribution for $x > 0:1$.

5. CONCLUSION

A "data set diagonalization" (DSD) procedure has been presented, which extends the Hessian method [1] for uncertainty analysis. The procedure identifies the directions in parameter space along which a given subset S of data provides significant constraints in a global fit. This allows one to test the consistency between S and the remainder of the data, and to discover which aspects of the fit are controlled by S .

The procedure involves "re-diagonalizing" χ^2 to obtain a new set of fitting parameters $fz_i g$ that are linear combinations of the original ones. The data from a given experiment or other chosen subset S of the data and its complement \bar{S} take the form of independent measurements of these new parameters, within the scope of the quadratic approximation. The degree

of consistency between S and \bar{S} can thus be examined by standard statistical methods.

The DSD method can be used to study the internal consistency of a global fit, by applying it with S defined by each experimental data set in turn. One can also let S correspond to subsets of the data that are suspected of being subject to some particular kind of unquantified systematic error. A full systematic study of the parton distribution fit using the new technique is currently in progress.

Typical applications of the new technique have been illustrated in the context of measuring parton distribution functions. The method uncovered and quantified tension between the two inclusive jet experiments, and between one of those experiments and the non-jet data, that was difficult to detect using the older methods, which are based on tracking the effect on χ^2 for S and \bar{S} in response to changing the weight assigned to S [4, 7].

The DSD method can also be used to identify which features of the fit are controlled by particular experiments or other subsets of the data in a complex data set. As an example of this, the jet experiments were shown to be the principal source of information on the gluon distribution in the region displayed in Fig. 4. The logic is as follows: Fig. 4 shows that the uncertainty of the gluon distribution is dominated by eigenvector directions 1 and 2 when S is defined as the jet data; and the range of acceptable fits along those directions is constrained mainly by the jet data according to Fig. 2 or Table V.

Acknowledgments

I am grateful to my late colleague and friend W u-K i Tung for the pleasure of many discussions on these issues. This research was supported by National Science Foundation grant PHY-0354838.

Appendix: Rediagonalizing the Hessian matrix

This Appendix describes details of the procedure that simultaneously diagonalizes the coordinate dependence of χ^2 and one additional quantity within the quadratic approximation. The procedure was first described in Appendix B of [7], but its significance was not recognized in that paper.

The Hessian method is based on the quadratic expansion of χ^2 in the neighborhood of the minimum

that defines the best fit to the data:

$$\chi^2 = \chi_0^2 + \sum_{i=1}^N \sum_{j=1}^N H_{ij} x_i x_j; \quad (12)$$

where x_i is the displacement $a_i - a_i^{(0)}$ from the minimum in the original parameter space, and the Hessian matrix is defined by

$$H_{ij} = \frac{1}{2} \frac{\partial^2 \chi^2}{\partial x_i \partial x_j} \bigg|_0; \quad (13)$$

(The Hessian matrix is usually defined without the overall factor $1/2$, but the normalization used here is more convenient for present purposes.) Eq. (12) follows from Taylor series in the neighborhood of the minimum. It contains no first-order terms because the expansion is about the minimum, and terms smaller than second order have been dropped according to the quadratic approximation.

Since H is a symmetric matrix, it has a complete set of N orthonormal eigenvectors $V_i^{(1)}; \dots; V_i^{(N)}$:

$$\sum_{j=1}^N H_{ij} V_j^{(k)} = \lambda_k V_i^{(k)} \quad (14)$$

$$\sum_{k=1}^N V_k^{(i)} V_k^{(j)} = \delta_{ij} \quad (15)$$

$$\sum_{k=1}^N V_i^{(k)} V_j^{(k)} = \delta_{ij}; \quad (16)$$

The eigenvalues λ_k are positive because the best fit must be at a minimum of χ^2 . Multiplying (14) by $V_m^{(k)}$ and summing over k yields

$$H_{ij} = \sum_{k=1}^N \lambda_k V_i^{(k)} V_j^{(k)}; \quad (17)$$

We can define a new set of coordinates y_j that describe displacements along the eigenvector directions:

$$S_j = \frac{1}{\sqrt{\lambda_j}} y_j \quad (18)$$

$$W_{ij} = V_i^{(j)} S_j \quad (19)$$

$$x_i = \sum_{j=1}^N W_{ij} y_j; \quad (20)$$

Then

$$\chi^2 = \chi_0^2 + \sum_{i=1}^N y_i^2; \quad (21)$$

Any additional function G of the original coordinates $f_{a_i}g$ can also be expressed in terms of the new coordinates $f_{z_i}g$ and expanded by Taylor series through second order:

$$G = G_0 + \sum_{i=1}^N P_i Y_i + \sum_{i=1}^N \sum_{j=1}^N Q_{ij} Y_i Y_j : \quad (22)$$

The symmetric matrix Q , like H , has a complete set of orthonormal eigenvectors $U_i^{(1)}; \dots; U_i^{(N)}$:

$$\sum_{j=1}^N Q_{ij} U_j^{(k)} = \lambda_k U_i^{(k)} \quad (23)$$

$$\sum_{k=1}^N U_k^{(i)} U_k^{(j)} = \delta_{ij} \quad (24)$$

$$\sum_{k=1}^N U_i^{(k)} U_j^{(k)} = \delta_{ij} ; \quad (25)$$

from which it follows that

$$Q_{ij} = \sum_{k=1}^N \lambda_k U_i^{(k)} U_j^{(k)} : \quad (26)$$

Defining new coordinates $f_{z_i}g$ by

$$z_i = \sum_{j=1}^N U_j^{(i)} Y_j \quad (27)$$

now leads to

$$\begin{aligned} \chi^2 &= \chi_0^2 + \sum_{i=1}^N z_i^2 \\ G &= G_0 + \sum_{i=1}^N \frac{1}{2} \lambda_i z_i^2 + \sum_{i=1}^N \sum_{j=1}^N \frac{1}{2} \lambda_i z_i^2 ; \end{aligned} \quad (28)$$

where

$$\lambda_i = \frac{1}{2} \sum_{j=1}^N U_j^{(i)} P_j : \quad (29)$$

Hence both χ^2 and G are diagonal in the new coordinates $f_{z_i}g$ in the quadratic approximation. Eq. (5), which is the basis of this paper, follows immediately from (28) by choosing G to be the contribution to χ^2 from the subset S of the data.

Because non-quadratic behavior appears at widely different scales in different directions of the original parameter space, and because the second-derivative matrices are calculated numerically by finite differences,

it is actually necessary to compute the linear transformation from the old coordinates $f_{a_i} a_i^{(0)}g$ to the new coordinates $f_{z_i}g$ by a series of iterations [8]. This is done as follows. The procedure described above yields a coordinate transformation W defined by

$$a_i - a_i^{(0)} = \sum_{j=1}^N W_{ij} z_j : \quad (30)$$

The coordinates $f_{z_i}g$ can be treated as "old" coordinates and the above steps repeated to obtain a refined set of elements for the matrix W . This process is iterated a few times to obtain the final form of the transformation. The iterative method is simple to program: each iteration begins with an estimate of the desired transformation matrix W in (30) and ends with an improved version of W . One can start with the unit matrix $W_{ij} = \delta_{ij}$ and iterate until the matrix W stops changing. This procedure has been found to converge in all of the applications for which it has been tried.

The distance moved away from the minimum in the original coordinate space is given by

$$D = \sum_{i=1}^N (a_i - a_i^{(0)})^2 = \sum_{i=1}^N \sum_{j=1}^N \sum_{k=1}^N W_{ki} W_{kj} z_i z_j ; \quad (31)$$

which corresponds to the choice

$$Q_{ij} = \sum_{k=1}^N W_{ki} W_{kj} \quad (32)$$

in the iterative scheme. This choice produces eigenvector directions that are characterized by how rapidly χ^2 changes in the original parameter space, leading to a clear distinction between "steep directions" in which χ^2 increases rapidly with displacement in the original parameters, and "flat directions" in which the χ^2 increases only slowly. The degree of steepness or flatness is measured by the eigenvalues of Q .

In the PDF analysis, a large number of free parameters are used in order to reduce the "parameterization error" caused by the need to represent unknown continuous parton distribution functions by approximations having a finite number of parameters. In that application, the logarithms of the eigenvalues of Q are found to be roughly uniformly distributed, with the smallest and largest eigenvalues having a huge ratio. As a result, the iterative method has been found to be necessary even to carry out the conventional Hessian analysis, where only χ^2 needs to be diagonalized.

-
- [1] J. Pumplin et al., Phys. Rev. D 65, 014013 (2001) [arXiv:hep-ph/0101032];
- [2] D. Stump et al., Phys. Rev. D 65, 014012 (2001) [arXiv:hep-ph/0101051].
- [3] P. M. Nadolsky et al., Phys. Rev. D 78, 013004 (2008) [arXiv:0802.0007 [hep-ph]].
- [4] J. Pumplin, J. Huston, H. L. Lai, W. K. Tung and C. P. Yuan, "Collider Inclusive Jet Data and the Gluon Distribution," [arXiv:0904.2424 [hep-ph]].
- [5] A. D. Martin, W. J. Stirling, R. S. Thorne and G. Watt, arXiv:0901.0002 [hep-ph].
- [6] The sum of quadratic deviations in Eq. (1) is the natural measure of fit quality if the experimental errors are Gaussian-distributed. If they are not Gaussian, alternative forms might be worth considering in which extreme values of the deviation $(D_i - T_i) = E_i$ are assigned more weight (e.g., $\chi^2 = \sum_i \frac{1}{E_i^4}$) to force the fit toward describing every data point satisfactorily; or more likely less weight (e.g., $\chi^2 = C \sum_i \log(1 + \frac{1}{E_i^2})$) to downplay the influence of extreme outlying points.
- [7] J. C. Collins and J. Pumplin, "Tests of goodness of fit to multiple data sets," arXiv:hep-ph/0105207.
- [8] J. Pumplin, D. R. Stump and W. K. Tung, Phys. Rev. D 65, 014011 (2001) [arXiv:hep-ph/0008191].
- [9] G. Moreno et al., Phys. Rev. D 43, 2815 (1991).
- [10] T. Aaltonen et al. [CDF Collaboration], Phys. Rev. D 78, 052006 (2008) [arXiv:0807.2204 [hep-ex]].
- [11] V. M. Abazov et al. [D0 Collaboration], Phys. Rev. Lett. 101, 062001 (2008) [arXiv:0802.2400 [hep-ex]].